Palaeogeography, Palaeoclimatology, Palaeoecology 307 (2011) 168–176

Contents lists available at ScienceDirect

Palaeogeography, Palaeoclimatology, Palaeoecology

journal homepage: www.elsevier.com/locate/palaeo

Patterns of local and regional grain size distribution and their application to Holocene climate reconstruction in semi-arid Inner Mongolia, China

Yi Yin, Hongyan Liu *, Siyuan He, Fengjun Zhao, Jiangling Zhu, Hongya Wang, Guo Liu, Xiuchen Wu

College of Urban and Environmental Sciences, and MOE Laboratory for Earth Surface Processes, Peking University, Beijing, 100871, China

ARTICLE INFO

Article history:
Received 14 April 2010
Received in revised form 4 May 2011
Accepted 7 May 2011
Available online 24 May 2011

Keywords:
Grain size
Lacustrine sediment
Aeolian activity
Palaeoenvironmental reconstruction
Semi-arid region
Northern China

ABSTRACT

The semi-arid temperate steppe in northern central China is one of the main areas influenced by frequent dust and sand storms, and is at the same time a primary source of dust from deteriorated grasslands; thus, the sediment grain size distribution of inland lakes in this region can be a particularly useful indicator of palaeoenvrionmental change. The local pattern of grain size suggests that aeolian activity is the most important agent for sedimentation in the lake center in this region, as strong northwesterly winds prevail for most of the year and the surface runoff is very weak. Meanwhile, the regional pattern of topsoil grain size and its close association with mean annual precipitation (MAP) allows the establishment of a statistical model for palaeo-moisture reconstruction from sediment grain size. In this study, we reconstructed a humidity time series based on the sediment grain size sequence from Anguli Nuur Lake on the southern Inner Mongolian Plateau in China and found that it coincides very closely with the C/N ratio (carbon to nitrogen ratio) and other humidity indices revealed in previous studies of this temperate steppe region and from the $\delta^{18}O$ values of stalagmite calcite in southern, monsoon-dominated China. This close relationship suggests that climate change in the semi-arid areas of Asia is strongly influenced by the Pacific summer monsoon and that it is reasonable to use sediment grain size as an indicator of humidity variability in the semi-arid steppe region. The reconstructed humidity increased during the early Holocene, and generally humid conditions lasted from about 10,400 until 7000 yr BP. The period from around 7000 to 5200 yr BP was a transition phase from humid to semi-arid conditions, and the monsoon intensity of that time may have been at the threshold for a semi-arid vegetation ecosystem. Finally, since approximately 5200 yr BP to present, the climate has become more arid, with corresponding vegetation deterioration and strong aeolian activity.

1. Introduction

The semi-arid temperate steppe on the central Inner Mongolian Plateau lies at the margin of Pacific monsoon influence, and is very sensitive to climate change since limited water availability constrains vegetation growth. It is one of the main areas to be influenced by frequent dust and sand storms in winter and spring, and is at the same time a primary source of dust from deteriorated grasslands (Wang et al., 2004; Lu et al., 2005). The dust, originating from the Inner Asian desert and deteriorated steppe, can be transported over a very long distance during winter and spring (*e.g.* to Japan, Iwasaka et al., 1983; Taiwan, Lin, 2001; and Alaska, Yasunari and Yamazaki, 2009); it is even likely to be a significant contributor to the deep-sea sediments of the North Pacific at mid-latitudes beneath the prevailing westerly winds (Duce et al., 1980; Bishop et al., 2002). The inland lake sediments have preserved abundant information about previous environmental change, and grain size in particular could be of great use given the strong aeolian transport in this semi-arid region. Mid-latitude semi-arid regions in Inner Asia are experiencing increasing drought due to temperature rise (IPCC, 2007), which is likely to have a profound influence on vegetation growth (Breshears et al., 2005; Allen et al., 2010). Thus, analysis of palaeo-environmental data is essential to understand the sensitivity of vegetation to modern climate dynamics and to predict future trends.

Grain size has been commonly used as an indicator of palaeo-climate change, mostly to indicate water erosion intensity in humid regions where coarse particles indicate increased precipitation (Wang et al., 1990; Chen et al., 2000, 2003; Wu et al., 2006), and to indicate wind erosion intensity in arid and semi-arid regions where coarse particles indicate lake shrinkage (De Deckker et al., 1991; Porter and An, 1995; Qiang et al., 2007). However, the interpretation of grain size is difficult, changing from case to case, even for the same site (*e.g.* Jin et al., 2000; Peng et al., 2005), and largely depends on comparison with other indices, as there is a lack of knowledge about modern grain size patterns and processes. Therefore, a good understanding of modern grain size patterns and transportation characteristics can greatly support interpretation of grain size data in palaeoenviron-mental studies.

* Corresponding author. Fax: +86 10 62759319.
E-mail address: lhy@urban.pku.edu.cn (H. Liu).

0031-0182/$ – see front matter © 2011 Elsevier B.V. All rights reserved.
doi:10.1016/j.palaeo.2011.05.011

Topsoil grain size and mean annual precipitation (MAP) in the semi-arid steppe of China are significantly linked (Liu et al., 2008), and the particles eroded from surrounding topsoil constitute the materials transported into lake sediments. In general, lake sediments are transported by both wind and water; however, in this semi-arid temperate steppe region, surface runoff is very weak, while aeolian erosion is extremely strong (Ji et al., 2004). In aeolian deposition, the particle transport distance was shown to be determined more by dust grain size than by wind velocity (Pye, 1987, 1995; Tsoar and Pye, 1987). The resulting distinct pattern of a substantial decrease in sand content in loess deposition over short downwind distances is therefore due to the source-to-deposit transport distance of sand-sized particles, rather than the effect of wind intensity (Ding and Sun, 1999; Ding et al., 2001, 2005; Yang and Ding, 2008). Thus, lake sediment grain size can be greatly influenced by the grain size distribution of the source materials, which in turn is closely linked to climate. Meanwhile, higher precipitation supports denser vegetation, which acts to reduce both wind and water erosion (Shi et al., 2004), preventing coarse grains from entering the lake. Therefore, we hypothesize that grain size changes can potentially serve as an indicator of palaeo-moisture variability, with coarser grains indicating a more arid environment, and vice versa, in semi-arid regions.

In this study, two different sediment sample types were investigated: one sample set was of topsoil from a large region across the woodland-steppe ecotone with a decreasing southeast-northwest MAP gradient, collected for analysis of the relationship between regional grain size pattern and MAP; the second sample set was of surface sediment from a specific desiccated lake (Anguli Nuur) and its surroundings, analyzed to recover the characteristics of particle transportation. The aim of the study was to improve the usage of grain size as an indicator of palaeoenvrionmental change, and to quantitatively reconstruct Holocene moisture changes in the semi-arid region of China.

2. Study area and sample sites

Our study area (41°18′–43°55′N, 110°47′–117°30′E) is located in the central part of the Chinese Inner Mongolian Plateau (Fig. 1a, b). Present climatic conditions are dominated by the winter monsoon from continental Inner Asia and the Pacific summer monsoon from the southeast; as a result, the waxing and waning of the Pacific monsoon controls the quantity of precipitation and the horizontal migration of vegetation zones over long time scales. A strong northwesterly wind prevails in winter and spring and is accompanied by frequent sand and dust storms. The vegetation pattern changes from woodland and shrubland (MAP>~400 mm), to meadow steppe (MAP ~400–350 mm), to typical steppe (MAP ~350–250 mm), and then to desert steppe (MAP ~250–150 mm) following a precipitation gradient which declines from southeast to northwest. However, there is no such obvious gradient in modern mean annual temperature (MAT) or mean July temperature; thus the humidity pattern is mainly controlled by precipitation availability. The most frequent community

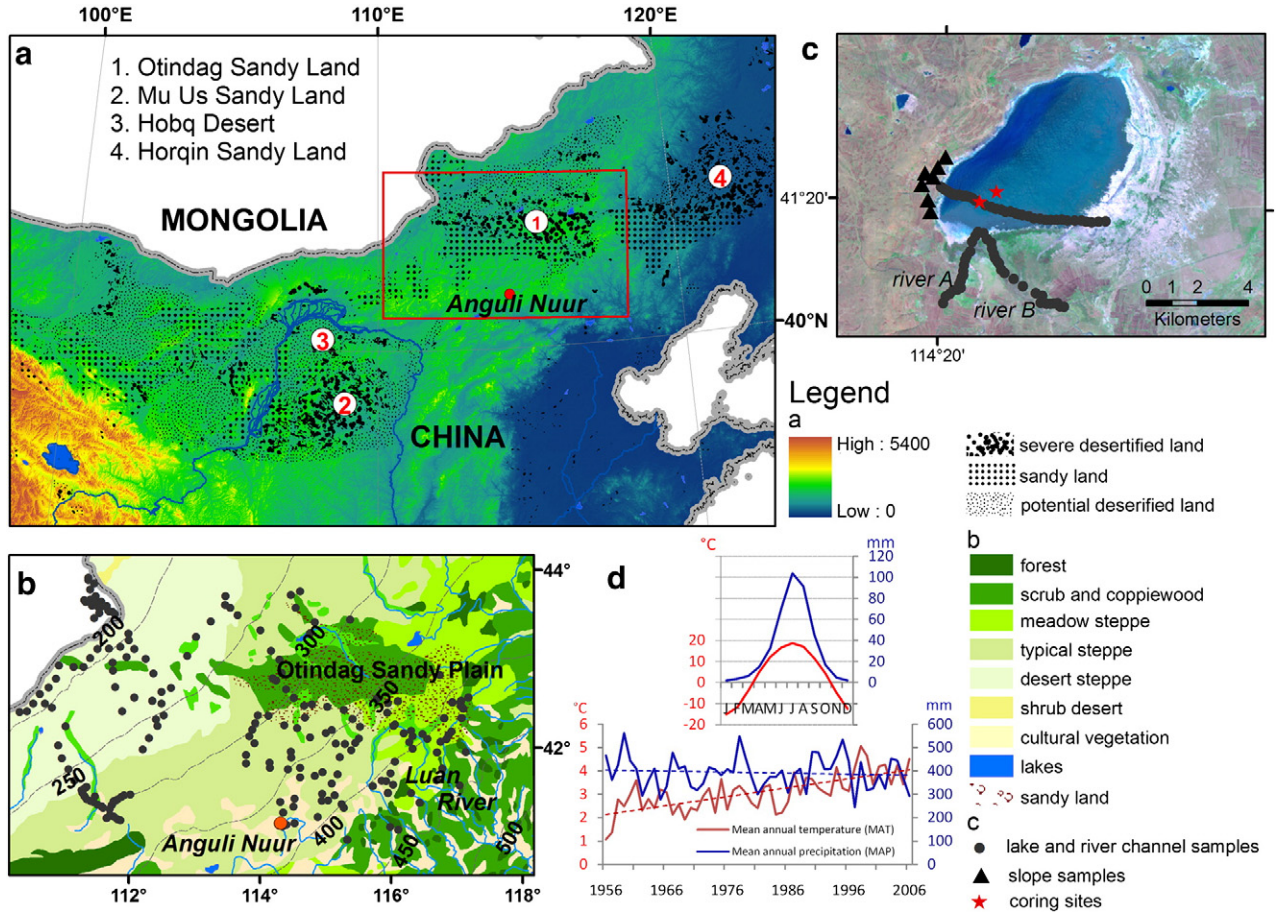

Fig. 1. (a) Topography of north-central China, with the location of our study area (red rectangle), the lake site (red dot), and distribution of deserts and sandy plains in and around this area (1–4); (b) study area showing topsoil sampling sites, vegetation patterns, and mean annual precipitation isohyets; (c) Anguli Nuur lake surface and river channel sampling sites (grey dots), slope deposit samples (triangle) and coring locations (stars); (d) average monthly precipitation (blue) and monthly temperature (red); trends in mean annual precipitation (blue) and mean annual temperature (red) in the last 50 years (1956–2006) at Zhangbei Meteorological Station, 40 km from Anguli Nuur.

types in the woodland zone are dominated by *Betula platyphylla*, *Betula dahurica*, *Quercus mongolica*, and *Pinus tabulaeformis*. Meadow steppe is dominated by *Stipa baicalensis* and *Filifolium sibiricum* along with abundant forb species. Typical steppe is dominated by *Stipa grandis, Stipa krylovii* and *Leymus chinensis*. The dominant species of the desert steppe are *Stipa gobica* and *Stipa glareosa*, accompanied by some shrubs such as *Salsola passerina* and *Reaumuria soongorica* from the desert zone.

Anguli Nuur ("Nuur" means "lake" in Mongolian; ~41°20′N, ~114°20′E; 1315 m altitude) is a saline inland lake, located at the southern-central edge of the Inner Mongolian Plateau (Fig. 1c), and occupying a shallow depression with a flat floor between small rolling basalt hills formed during the Late Miocene epoch. The MAT is 3.1 °C; the MAP is 392 mm, 60–70% of which occurs in summer; the mean annual evaporation is 1956 mm; evaporation greatly exceeds precipitation and most precipitation is exhausted by evaporation; the mean annual runoff is less than 10 mm, and the mean annual water yield is 0.74 mm, as indicated by records from the Zhangbei Meteorological Station and Water Bureau of Zhangbei (1956–2006, Fig. 1d). In 1986 the lake had a water surface area of around 40 km^2, a maximum depth of about 4 m, and a drainage area of 722.4 km^2 (Wang and Dou, 1998). Remote sensing data have revealed that the water surface area has been highly variable over the last 40 years, largely reflecting the balance between precipitation and evaporation (Zhang, 2010). The lake was totally desiccated in 2004, probably because of low precipitation from 1997 to 2000, evaporation increases induced by warming, and groundwater exploitation (Water Bureau of Zhangjiakou City, 2005; Zhang, 2010). The lake catchment is hydrologically closed, and the inflow rivers are seasonal, with small inflow volumes. There has been no major geologic movement since the Late Miocene at our study site (Qiu et al., 1999) and the catchment settings have not changed greatly during the Holocene. The lake surface is ice covered from mid-October until March or April, and during that time a strong northwesterly wind prevails. The mean monthly wind velocity ranges from 2.8 m/s in December to 4.8 m/s in April. The wind is stronger than 10.8 m/s for 50 to 70 days/year, with frequent sandstorms (Qiu et al., 1999; Zhai et al., 2006). There are no large scale fisheries, reed cutting, or agricultural activities in the lake basin, as the lake is strongly saline and alkaline, and the population density of the area is relatively low (Water Bureau of Zhangbei, 2005).

3. Materials and methods

3.1. Field investigation and sampling

Two different sediment sample types were investigated. One sample set of topsoil (174 samples comprising 31 from woodland, 19 from meadow steppe, 93 from typical steppe, and 31 from desert steppe) was collected systematically from a wide region across the woodland-steppe ecotone to analyze the relationship between regional grain size patterns and MAP (Fig. 1b); another sample set of surface sediments was collected from a desiccated lake (Anguli Nuur) and its surroundings (47 samples of 0–5 cm deposits from dry lake surface sediments along a northwest to southeast transect across the lake basin, 21 samples from lakeshore slopes, and 31 samples from two inflow river channel deposits) to recover the characteristics of particle transportation (Fig. 1c). Sampling sites were selected to represent the most typical conditions for each vegetation or sediment type group, avoiding obvious human disturbance, wind ripples, severely eroded areas and other disturbances. Grain sizes of riverbed sediment showed some lateral variation, changing along a moderate gradient from the middle of the river channel to the river bank. For the analysis we chose samples from the middle of the river channel, where water velocity was generally greatest. In addition, plant abundance, cover, and height of each species, as well as habitat features, including altitude, slope, aspect and land use type, were recorded for each 2 m by 2 m plot selected for the regional topsoil samples and local catchment slope samples.

Two parallel sediment cores (An-S: 1138 cm long and An-C: 870 cm long) were extracted in 2005 using a gravity corer, and were sub-sampled into 1 cm discs for further measurements. A third core, An-A, focusing on the upper 135 cm section, was extracted from near the former coring position and was sub-sampled into 5 mm discs in 2007 to provide supplementary material. In this paper, we have mainly focused on core An-S.

3.2. Chronological analysis

The chronology of the sediment cores was defined by AMS ^{14}C dating and ^{210}Pb and ^{137}Cs activity analysis. AMS ^{14}C dating of all three cores was performed in the AMS Laboratory of Peking University. Samples from depths where sediment texture displayed slight changes were dated. All dates were calibrated to calendar years before present (cal yr BP) with OxCal v3.10, using the IntCal04 calibration data set (Reimer et al., 2004). In saline lake environments, the reservoir effect is frequently the most important artifact prohibiting accurate carbon dating (Ren, 1998; Geyh et al., 1999), so supplementary samples of the upper 20 cm from An-A were taken to conduct ^{210}Pb and ^{137}Cs activity analysis; a total of 40 slices (0– 20 cm) were analyzed for ^{210}Pb activity and 20 slices (0–10 cm) for ^{137}Cs activity using a gamma spectrometer at the Environmental Radiochemistry Laboratory in the Chinese Academy of Agricultural Sciences. Ages in the top sections were determined according to the Constant Rate of Supply (CRS) model (Binford, 1990), after taking ^{137}Cs activity peak values into consideration. The age–depth relationship between An-S and An-A was established by correlations between their grain size and total organic carbon (TOC) profiles (details are available in Wang et al., 2010). We then integrated the ages shown by the CRS model and by the AMS ^{14}C dating and validated our ^{14}C age model by comparing the An-S profile with laminar ages presented by Zhai and Li (2002); Zhai et al. (2006), based on the correlation with abrupt grain size shifts (Wang et al., 2010).

3.3. Laboratory measurements

The grain size distribution of all samples was analyzed using a Malvern Mastersizer 2000, which has a measurement range of 0.02–

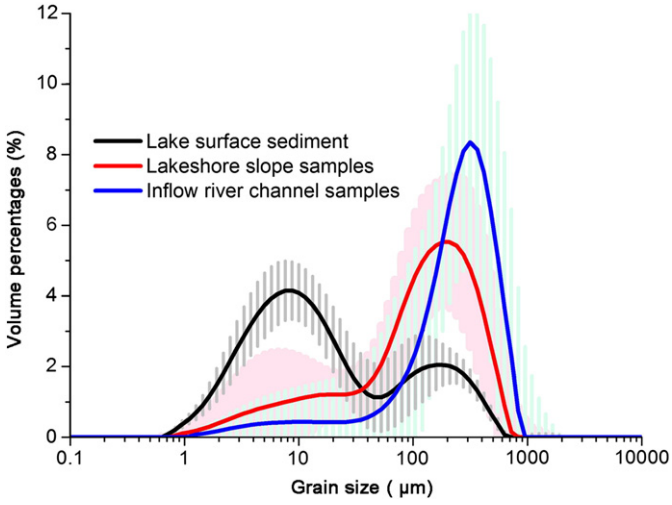

Fig. 2. Grain size distributions of the three different sediment types: lake surface sediments, river channel deposits, and catchment slope deposits; the shadows show the standard variations.

2000 μm. Samples were repeatedly pretreated with 10–20 ml of 30% H_2O_2 until no further bubbles were produced, to remove organic matter, and then boiled with 10 ml of 10% HCl to remove carbonates. About 400 ml deionized water was added and the sample solution was kept for 12 h to rinse acidic ions, then the upper clear water layer was siphoned off. This step was repeated at least 3 times until the pH value was close to 7. The sample residue was finally boiled with 10 ml of 0.5 mol/L $(NaPO_3)_6$ and treated on an ultrasonic vibrator for 30 s before testing by Malvern Mastersizer 2000 within 3 h after cooling. TOC and total nitrogen (TN) were analyzed by an Elementar Vario EL (Germany) after removal of roots and other macro organic remains, and ground to pass through a 149 μm soil sieve.

3.4. Statistical model for the relationship between topsoil grain size and MAP

In order to avoid human influence on vegetation and soil, we selected sites with minimal human disturbance, based on species composition (human disturbance index (HDI) <1.8, Liu et al., 2006, 2008). Sites located in the Otindag Sandy Plain were rejected for the statistical model, as they have quite different soil parent materials from the other relatively uniform weathering materials of granite. Thus we assumed that climate is a crucial control on the regional grain size pattern through its effects on not only vegetation cover but also on soil development, micro-organism activity and erosion.

Climatic records from 1956 to 2006 from 50 stations within and around the study area were collected to interpolate the spatial pattern of MAP using the Kriging method. An artificial neural network (ANN) was adopted to provide a convenient and powerful means of performing nonlinear classification and regression (Skapura, 1996; Van der Baan and Jutten, 2000). We divided the particle distributions into 14 size fractions: C_1 (<1 μm), C_2 (1–2 μm), C_3 (2–5 μm), C_4 (5–10 μm), C_5 (10–20 μm), C_6 (20–30 μm), C_7 (30–40 μm), C_8 (40–50 μm), C_9 (50–63 μm), C_{10} (63–100 μm), C_{11} (100–250 μm), C_{12} (250–500 μm), C_{13} (500–1000 μm) and C_{14} (>1000 μm) to build the input matrix, and defined MAP as the target matrix during back-propagating (BP) neural network construction and training. The BP neural network was implemented in MATLAB. We used the Levenberg–Marquardt algorithm to train the net, and the mean squared error to estimate the performance. Comparison with traditional statistical methods, such as multiple linear regression and principal component regression, was also conducted to validate the performance of the BP neural net work.

3.5. Palaeo-moisture reconstruction and validation

The modern spatial relationship between grain size and MAP constructed by the BP neural network was next used to establish temporal variations, using lake sediment from the semi-arid region of China. It must be stressed that the relationship between modern topsoil grain size and MAP was established when there was no significant modern MAT gradient, which means precipitation mainly determined the moisture status; however, changes in both temperature and precipitation have strong influences on the palaeoenvironment, so there are considerable risks in attributing the shifts directly to precipitation changes. In addition, the linkage between surface soil characteristics and sediment through transportation and sorting is very complicated. Consequently, it is very difficult to validate the absolute value of the reconstructed MAP; however, relative trends can be reliably obtained. Therefore, we conducted a systematic calibration to create a relative humidity index (RHI), ranging from 0 to 1, based on reconstructed MAP from the BP neural network, to show the relative humidity changes through time.

Two additional indices from other studies have been cited here for comparison: one is the synthesized four-class ordinal wetness index (WI) from a review of 6 sites in the temperate steppe zone in north-central China (Zhao et al., 2009; Fig. 5e); the other is the $\delta^{18}O$ record from stalagmite calcite in the Dongge Cave in southern China, indicating the Asian summer monsoon intensity (Dykoski et al., 2005; Fig. 5e). Other indices for the same profile An-S, including pollen and magnetism characteristics, were also considered when analyzing the moisture changes through the Holocene (Liu et al., 2010; Wang et al., 2010).

4. Results

4.1. Regional topsoil grain size distribution and its relationship with MAP

The correlation between top soil sand fraction (>63 μm) and MAP was significant at the 0.01 level (2-tailed), with a correlation coefficient of −0.586: the higher the precipitation, the lower the sand fraction. Woodland and meadow steppe soils with higher precipitation had the highest clay and lowest sand fractions, while desert steppe soils had the lowest clay fraction and the highest sand fraction (Table 1). Variations in clay fractions in all vegetation types were much higher than those in other fractions.

The BP neural network, which was constructed from the topsoil grain size matrix and MAP matrix, achieved a better fit between the simulated and observed data than that of the multiple linear regression or principal components analysis. The R^2 of the training set reached 0.99 (the training set was a random sub-sample of 70% of the total sample set: $n=119$); the R^2 of the validation and test sets reached 0.81 and 0.77, respectively (with 15% sub-sample sizes in each case). Overall the R^2 was 0.90, suggesting that the output could explain most of the variation in the 14 grain size groups, and thereby demonstrating that it is reasonable to use the BP neural network to reconstruct the past humidity changes.

4.2. Local patterns of grain size distribution

Fig. 2 shows the typical grain size distribution curves of the three different sediment types: dry lake surface sediment, river channel deposit, and catchment slope topsoil. The main peak of the frequency distribution of river channel deposits was at around 300 μm, while that of the catchment slope samples was at around 200 μm. The mean grain size of lake surface samples was much smaller, and the size distribution curves showed two peaks in most cases, at around 10 and around 200 μm. The volumetrically weighted averages in grain size fractions of samples taken along two inflow rivers and from the lake surface all showed a notable decreasing trend from the lake shore to the centre (Fig. 3). The fractions of >250 μm particles also showed the same decreasing pattern. However, following the sharp decrease in the coarse particle fraction after entering the lake, the volumetrically weighted averages became relatively stable.

Table 1
Mean values and coefficients of variation (inside the brackets) of MAP, vegetation coverage and grain size fractions in different vegetation types.

	Woodland (mainly *Betula* forest patches)	Meadow steppe	Typical steppe	Desert steppe
Sample number	31	19	93	31
Average MAP	418.59 (0.08)	378.34 (0.02)	288.19 (0.20)	152.83 (0.13)
Average vegetation coverage	70%[a]	51.8%	32.6%	11.3%
Clay (<2 μm)	3.19 (0.40)	2.21 (0.94)	0.92 (2.09)	0.88 (0.63)
Silt (2–63 μm)	34.17 (0.25)	29.79 (0.48)	28.59 (0.48)	17.95 (0.50)
Sand (>63 μm)	62.64 (0.13)	68.00 (0.23)	70.49 (0.19)	81.17 (0.11)

[a] Vegetation coverage of undergrowth herbaceous layer.

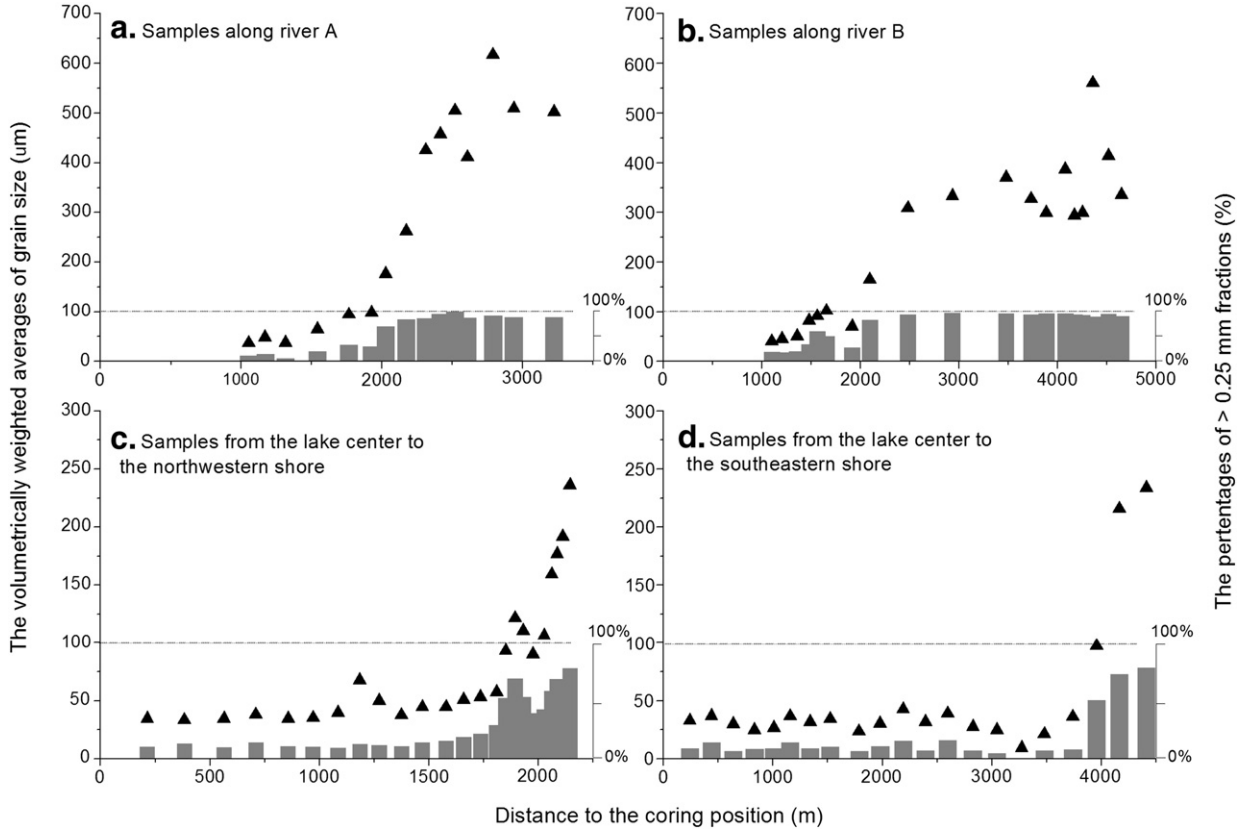

Fig. 3. Trends in volumetrically weighted averages (triangles) of grain size fractions at sites along a transect from lake shore to lake center and along the inflow-rivers and percentages of >250 μm particles (columns).

4.3. Profile characteristics and chronology results

The 1138 cm An-S section was mainly composed of clay and silt. Three zones were identified by visual inspection: the lower 58 cm and the upper 130 cm were silty clay; the middle part was mainly fine black clay. Salt crystal slices were found at the depths of 383–425, 450–460 and 495–529 cm, and white–dark laminations were found at the depth of around 560–800 cm. No hiatus was found for the whole section, thus we assumed that the sediment has not been strongly disturbed, even if it could have been seasonally desiccated during drought events.

Four bulk sediment samples from different sites on the lake surface provided calibrated ^{14}C AMS ages as follows: modern age (An-S 5 cm), 1870 cal yr BP (An-C 5 cm), 4245 cal yr BP (An-A 10 cm) and 4455 cal yr BP (An-A 20 cm) (Fig. 4b). However, ^{210}Pb and ^{137}Cs analysis results show that the surface 20 cm of An-A was composed of modern sediment (Fig. 4a). The apparent disagreement indicates the strong influence of the lake reservoir effect, which was site specific, fluctuating greatly through time and space, and depending on the proportions of the included organic matter, groundwater influence, exchange with atmospheric CO_2, and other factors. The lake aquatic system may have changed significantly through the Holocene. Thus, direct linear correction of the whole profile by simply subtracting the "old carbon" age may be potentially risky.

From 20 cm and below, the sedimentation rate calculated by the CRS model was equivalent to the rate calculated by the ^{14}C dates. The materials in the bottom section, along with even deeper sections which could not be extracted by gravity coring in the field as they were too loose, contained much more sand. Thus we assume that the ^{14}C age of these bottom sediments is consistent with the end of the Younger Dryas, which does not reveal a strong influence of the lake reservoir effect. Therefore, we decided to use ^{210}Pb and ^{137}Cs dating for the upper 20 cm, to avoid the strong "lake reservoir " effect in the upper section, and to allow linear interpolation between calibrated ^{14}C dates for the lower section without application of the lake reservoir effect correction as we do not know the exact influence.

Our chronology excluded two ^{14}C dates of pollen extractions from An-S (566 and 621 cm) in the lower section, which are not in reasonable agreement with other dates from both pollen extraction and bulk sediment samples from An-S and An-C. The deviation may be attributed to modern contamination or to random error due to the small sample size.

The grain size results supported the age model, including the dramatic increase in coarse partial fraction (>100 μm) percentages in the upper 130 cm (Fig. 4c). In addition, our dating coincides well with the radiocarbon and laminar ages of Zhai's profile for the corresponding depth at 129 cm and below, based on the correlation with abrupt grain size shifts. An integrated age model of the whole core was then constructed (Fig. 4b): according to this model, a constant sedimentation rate was apparent before 5 ka BP, and then the sedimentation rate became notably slower. However, it has to be acknowledged that this age model is not totally satisfactory.

4.4. Reconstructed Holocene humidity variation

In general, the reconstructed relative humidity index (RHI) coincided very well with the C/N ratio and the other two regional humidity indices (Fig. 5). The reconstructed RHI and C/N ratio both showed an increasing trend from the onset of the Holocene and then reached a relatively stable and high level by around 10,300 cal yr BP. These humid conditions persisted, with moderate fluctuations, until about 7000 cal yr BP; following this, the period around 7000–

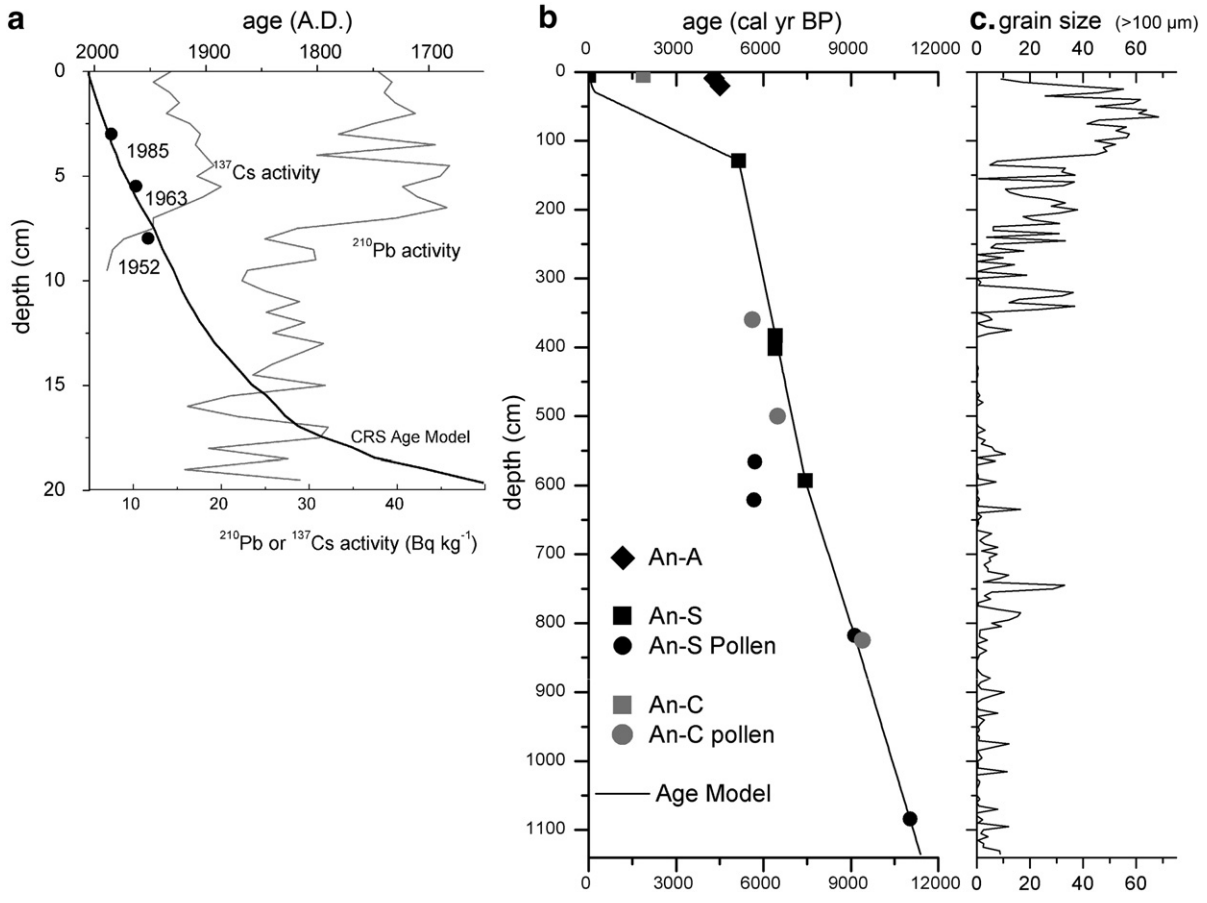

Fig. 4. (a) ^{210}Pb and ^{137}Cs age model; (b) age–depth relationship of the An-S profile; (c) variations of the grain size of >100 μm fractions in the An-S core.

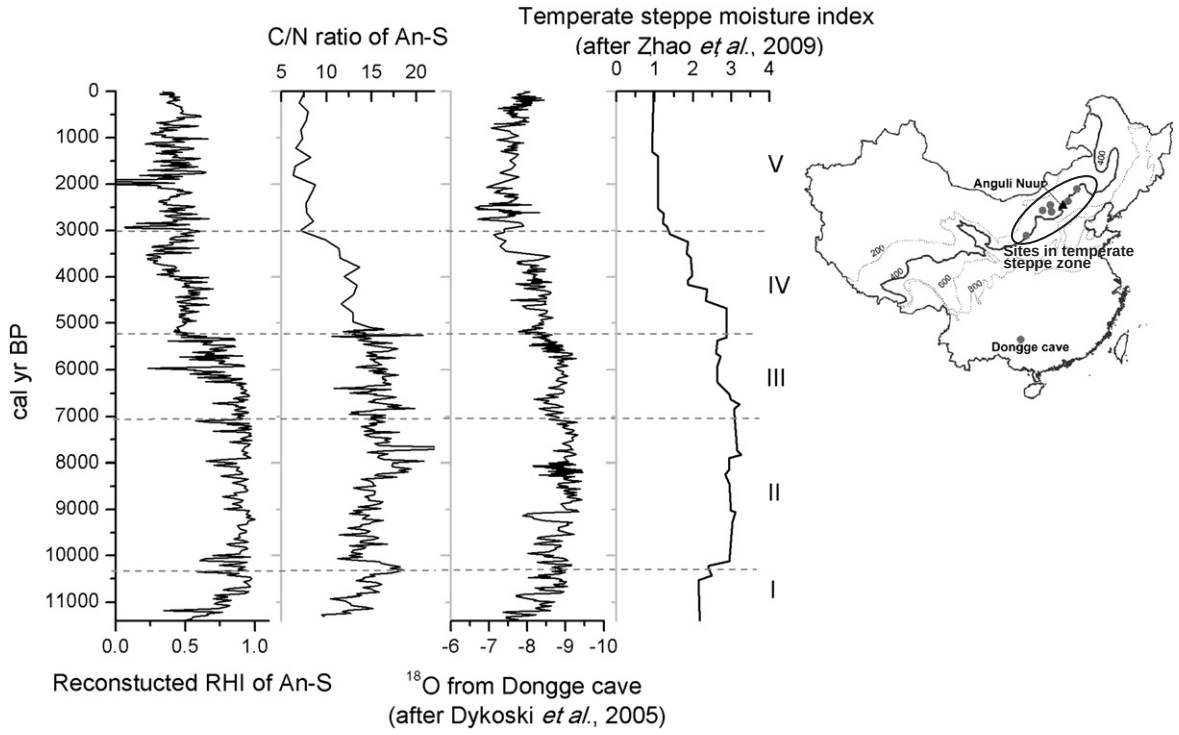

Fig. 5. Holocene moisture variability: (a) reconstructed relative humidity index (RHI) of Anguli Nuur (An-S) using variations in grain size; (b) the carbon to nitrogen ratio of An-S; (c) the δ^{18}O values from stalagmite calcite in Dongge Cave from southern China, indicating Asian monsoon precipitation (Dykoski et al., 2005); (d) synthesized four-class ordinal Wetness Index from a review of 6 sites in the temperate steppe zone in north-central China (Zhao et al., 2009); and (e) a map showing related locations (grey dots).

5200 cal yr BP was a transition phase from humid to dryer conditions. Finally, the humidity decreased to a significantly lower level. In total, five phases were distinguished by visual inspection, and are described below.

In phase I (11,400–10,300 cal yr BP), the RHI based on grain size increased prominently from 0.5 to 0.9, and C/N ratios rose from 10 to nearly 18. In phase II (10,300–7000 cal yr BP), the RHI was generally high and relatively stable (mean = 0.88, cv = 0.08), and the C/N ratios followed a generally increasing trend. In phase III (7000–5200 cal yr BP), the RHI in the first half of the period (7000–6400 cal yr BP) was stable and high (mean = 0.9, cv = 0.07), but the C/N ratio fluctuated markedly around a decreasing trend. During the latter half (6400 to 5200 cal yr BP), RHI decreased and showed strong fluctuations (mean = 0.69, cv = 0.24), and the C/N ratio decreased correspondingly. In phase IV (5200–3000 cal yr BP), following the last transitional stage, the RHI dropped to a significantly lower value (mean = 0.46, cv = 0.23), and accordingly the C/N ratio decreased markedly. In phase V (3000 cal yr BP–present), the RHI was low and highly variable (mean = 0.4, cv = 0.34). The RHI dropped to its lowest level at around 2000 cal yr BP. Meanwhile, the C/N ratio also became very low during this time(less than 8).

5. Discussion

5.1. Effect of climate on regional topsoil grain size patterns

The close relationship between the modern grain size pattern and MAP shows that climatic factors are the primary influence on regional topsoil grain size patterns, which can be explained by two main factors: vegetation characteristics and aeolian sorting.

The critical climatic constraint on vegetation growth in semi-arid areas is water availability (Bates et al., 2006), which mainly depends on precipitation; vegetation, in return, feeds back into climatic conditions. Vegetation together with its root systems and microorganism activities, also has a great influence on nutrient accumulation and soil development. Further, vegetation can protect fine grains from erosion (Hu et al., 1991), especially in areas where aeolian erosion is intense. In our study area, the prevailing wind direction coincides with the precipitation gradient (from northwest to southeast); the finer particles in the upper drift, which are vulnerable to erosion, could be transported and deposited in areas that are wetter or where the vegetation cover becomes denser.

Climatic factors also have a strong influence on aeolian activities. The influence of climate on aeolian activity depends not only on wind velocity but also on precipitation and temperature, which, in turn, determine evaporation (Shi et al., 2004). Vegetation reduces the wind velocity at the soil surface, and the relationship between vegetation coverage and wind erosion rate is an exponential function, i.e., the wind erosion rate decreases exponentially with increasing of vegetation coverage (Dong et al., 1987; Liu et al., 1992). Historical documentation of wind erosion and its disastrous consequences in China dates back over 2000 years and reveals that periods with frequent sand storms correspond to periods of a dry and cold climate (Zhang, 1984; Zhang and Lu, 1999). The frequency of strong and extreme dust storms has generally increased since the 1950s in Inner Mongolia, while records of mean wind velocity show a decreasing trend, which means that wind power, the direct driving force of aeolian activity, has not been the main factor increasing aeolian transport intensity; instead, the influences of precipitation and evaporation are likely causes (Zhang and Lu, 1999; Shi et al., 2001). In fact, wind intensity is not thought to have varied significantly during the past 5000 years (Küster et al., 2006; Nagashima et al., 2007). Therefore, the modern grain size–MAP relationship in the semi-arid region of China can be applied to the lake sediments in this region to reconstruct temporal climate variations.

5.2. Overwhelming contributions of aeolian activity to the coarse sand fraction in lake sediments

Aeolian activities are the most important agent controlling lake sedimentation in the semi-arid temperate steppe region, due to the strong northwesterly prevailing wind and very weak surface runoff. The differences in grain size components between the lakeshore slope, river channel and lake surface suggest that the lake sediments are a sink for the fine-grained particles produced elsewhere in the basin (Fig. 3; Xiao et al., 2009). Following the sharp decrease in coarse particles shortly after entering the lake (Fig. 4), the volumetrically weighted averages became relatively stable, which implies that runoff only has a prominent influence on particle transportation over a very short distance after entering the lake. Moreover, the trend from the northwestern shore to the center showed a more regular decrease in the coarse particle fraction than that from the southeastern shore to the center; the latter showed a slightly decreasing trend in the coarse sand fraction from the lake center to the shore before reaching the lakefront. This is consistent with aerodynamic sorting under the prevalent northwesterly wind, and supports the hypothesis concerning transport of coarse fractions by the wind.

Coarse sand fractions that have accumulated in the lake center are most likely carried there by strong winds through saltation and creeping over the ice cover that is present annually from mid October until March. During this period, strong winds carry coarse particles onto the ice. As the thermal capacity of these particles is less than that of ice, they heat up faster when exposed to sunlight and melt the ice beneath them. As a result, the particles become trapped in the ice on sunny days, and are then frozen into the ice at night. When the ice cover melts in spring, the coarse particles drop into the lake and are deposited on its bottom as sediment (Qiang et al., 2007). Previous studies of Anguli Nuur lake showed that grain size variations are a good indicator of winter monsoon strength during the Holocene (Zhai et al., 2006; Jiang et al., 2004), focused their investigation on the last 400 years, and reached the conclusion that wind-borne coarse particles contribute overwhelmingly to total sedimentation in the lake. A study of excess ^{210}Pb flux characteristics of the Anguli Nuur lake sediment also supports the result that aeolian activities dominate lake sediment input (Chen and Zhao, 2009).

5.3. Monsoon-dominated Holocene moisture changes in the semi-arid ecotone

The C/N ratio provides information about terrestrial vegetation biomass input and phytoplankton productivity, which is primarily constrained by water availability in the semi-arid temperate steppe (Fig. 5). The match between temporal variations in RHI and C/N ratio suggested that the reconstructed moisture time series is reasonably reliable. The δ^{18}O records from stalagmite calcite in the Dongge Cave in southern China (Dykoski et al., 2005) mainly indicate the influence of the Pacific Summer Monsoon, which brings most of the precipitation to our study area. The synthesized four-class ordinal wetness index (WI) obtained from the analysis of 6 sediment profiles in the temperate steppe zone (Zhao et al., 2009) illustrates the average regional moisture conditions during the Holocene.

All indices showed good general agreement in the early Holocene (Phase I, 11,400–10,300 cal yr BP) and point towards a humidity increase, probably caused by intensification of the Pacific Summer Monsoon as shown by the Dongge δ^{18}O values, and forced by low latitude insolation (Berger and Loutre, 1991). This intensification of the summer monsoon may have increased both precipitation and temperature in most parts of East Asia (An et al., 2000), including those in the mid-latitude semi-arid or even arid regions (Zhao et al., 2009), which promoted terrestrial vegetation growth at a continental scale. In phase II (10,300–7000 cal yr BP) all indices indicated persistent humid conditions, probably sustained by a strong summer

monsoon (with $\delta^{18}O$ values around −9‰). Pollen records from this site showed high arboreal pollen percentages (Liu et al., 2010), coinciding well with high terrestrial organic matter input as indicated by C/N ratios. In phase III (7000-6400 cal yr BP), there was an apparent disagreement in the first half of the period between the reconstructed high RHI and desertification indicated by salt crystals in the sediment; this could be explained by rising temperatures enhancing lake water evaporation, which would have led to severe drought events on a local scale. This result would also imply that the RHI is more sensitive to direct precipitation changes, and probably experiences a time lag with respect to abrupt environmental changes. Pollen analysis results showed a high percentage of *Ephedra* and *Nitraria* during that time, suggesting a more arid environment (Liu et al., 2010). Conditions during the latter half of phase III are consistent with delayed environmental deterioration after droughts. During this phase, the summer monsoon intensity did not show marked changes; however, the monsoon intensity of that time may have been close to the threshold for a semi-arid ecosystem interms of its water availability. In the following phases IV and V (5200 cal yr BP–present), all indices suggested a drier climate and the temperate steppe region became dramatically drier as shown by regional WI values. These results strongly suggest that the moisture evolution in this semi-arid area is mainly controlled by summer monsoon intensity, and that local extreme drought events could trigger nonlinear ecosystem deterioration.

6. Conclusions

Our results and discussion suggest that aeolian activities are the most important agent influencing sedimentation in the semi-arid temperate steppe region, which experiences a strong northwesterly prevailing wind and very weak surface runoff. The grain size distributions of surrounding source materials, and source area vegetation conditions, are two critical factors in determining the lake sediment grain size, and are both controlled by water availability, mainly through MAP. Climatic conditions (especially moisture) and vegetation coverage have stronger influences on aeolian activities than wind velocity. Thus, the modern spatial relationship between grain size and MAP can be used to estimate the temporal moisture conditions inferred from lake sediments in the semi-arid region in China.

The reconstructed humidity variations coincided very closely with the C/N ratio, as well as with other humidity indices obtained in previous studies of this temperate steppe region and from the $\delta^{18}O$ values of stalagmite calcite in southern, monsoon-dominated China. These close relationships suggest that climate change in semi-arid areas is strongly influenced by the Pacific summer monsoon and that it is reasonable to use sediment grain size as an indicator of humidity variability in the semi-arid steppe region. The reconstructed humidity increased from the beginning of the Holocene, and this generally humid period lasted from about 10,400 to 7000 cal yr BP. The period from around 7000 to 5200 cal yr BP was a transition phase from humid to semi-arid and arid conditions, and the monsoon intensity of that time may have been at the threshold for a semi-arid vegetation ecosystem. Since approximately 5200 yr BP, the climate has become more arid, in association with vegetation deterioration and strong aeolian activities.

Acknowledgements

This research was supported by a grant from the Natural Sciences Foundation of China (40771208 and 41071124). We are grateful to Mr. Qinglu Li and his staff for their help in coring sediments from Anguli Nuur, and Elisabeth Clement and Dave Chandler for their help in editing the text. We also thank the reviewers and editors, whose comments and suggestions have greatly improved the manuscript.

References

Allen, C., Macalady, A., Chenchouni, H., Bachelet, D., McDowell, N., Vennetier, M., Kitzberger, T., Rigling, A., Breshears, D., Hogg, E., 2010. A global overview of drought and heat-induced tree mortality reveals emerging climate change risks for forests. Forest Ecology and Management 259, 660–684.

An, Z.S., Porter, S.C., Kutzbach, J.E., Wu, X.H., Wang, S.M., Liu, X.D., Li, X.Q., Zhou, W.J., 2000. Asynchronous Holocene optimum of the East Asian monsoon. Quaternary Science Reviews 19, 743–762.

Bates, J., Svejcar, T., Miller, R., Angell, R., 2006. The effects of precipitation timing on sagebrush steppe vegetation. Journal of Arid Environments 64, 670–697.

Berger, A., Loutre, M., 1991. Insolation values for the climate of the last 10 million years. Quaternary Science Reviews 10, 297–317.

Binford, M., 1990. Calculation and uncertainty analysis of ^{210}Pb dates for PIRLA project lake sediment cores. Journal of Paleolimnology 3, 253–267.

Bishop, J.K.B., Davis, R.E., Sherman, J.T., 2002. Robotic observations of dust storm enhancement of carbon biomass in the North Pacific. Science 298, 817–821.

Breshears, D., Cobb, N., Rich, P., Price, K., Allen, C., Balice, R., Romme, W., Kastens, J., Floyd, M., Belnap, J., 2005. Regional vegetation die-off in response to global-change-type drought. PNAS 102, 15144.

Chen, Y.F., Zhao, Z.Z., 2009. Preliminary study on excess ^{210}Pb flux characteristic of lake sediment in arid regions and its implication for aeolian activity. Journal of Lake Sciences 21, 813–818 (in Chinese with English Abstract).

Chen, J.A., Wan, G.J., Tang, D., 2000. Recent climatic changes recorded by sediment grain sizes and isotopes in Erhai Lake. Progress in Natural Science 10, 54–61.

Chen, J.A., Wan, G.J., Zhang, F., 2003. Environment records of lake sediment under different time scales – case study of grain size. Science in China (Series D) 33, 563–568.

De Deckker, P., Correge, T., Head, J., 1991. Late Pleistocene record of cyclic eolian activity from tropical Australia suggesting the Younger Dryas is not an unusual climatic event. Geology 19, 602–605.

Ding, Z.L., Sun, J.M., 1999. Changes in sand content of loess deposits along a North–South transect of the Chinese Loess Plateau and the implications for desert variations. Quaternary Research 52, 56–62.

Ding, Z.L., Yu, Z.W., Yang, S.L., Sun, J.M., Xiong, S.F., Liu, T.S., 2001. Coeval changes in grain size and sedimentation rate of eolian loess, the Chinese Loess Plateau. Geophysical Research Letters 28, 2097–2100.

Ding, Z.L., Derbyshire, E., Yang, S.L., Sun, J.M., Liu, T.S., 2005. Stepwise expansion of desert environment across northern China in the past 3.5 Ma and implications for monsoon evolution. Earth and Planetary Science Letters 237, 45–55.

Dong, G.R., Li, C.Z., Jin, J., Gao, S.Y., Wu, D., 1987. Some results from wind erosion experiments by wind tunnel. Chinese Science Bulletin 32, 297–301.

Duce, R., Unni, C., Ray, B., Prospero, J., Merrill, J., 1980. Long-range atmospheric transport of soil dust from Asia to the tropical North Pacific: temporal variability. Science 209, 1522.

Dykoski, C., Edwards, R., Cheng, H., Yuan, D., Cai, Y., Zhang, M., Lin, Y., Qing, J., An, Z., Revenaugh, J., 2005. A high-resolution, absolute-dated Holocene and deglacial Asian monsoon record from Dongge Cave, China. Earth and Planetary Science Letters 233, 71–86.

Geyh, M., Grosjean, M., Núnez, L., Schotterer, U., 1999. Radiocarbon reservoir effect and the timing of the late-glacial/early Holocene humid phase in the Atacama Desert (northern Chile). Quaternary Research 52, 143–153.

Hu, M.C., Liu, Y.Z., Wu, L., Yang, Z.T., Wu, D., 1991. An experimental study in wind tunnel on wind erosion of soil in Korqin Sandy Land. Journal of Desert Research 11, 22–29 (in Chinese with English abstract).

IPCC, 2007. Climate Change 2007: Synthesis Report. In: Core Writing Team, Pachauri, R. K., Reisinger, A. (Eds.), Contribution of Working Groups I, II and III to the Fourth Assessment Report of the Intergovernmental Panel on Climate Change. IPCC, Geneva, Switzerland.

Iwasaka, Y., Minoura, H., Nagaya, K., 1983. The transport and spacial scale of Asian dust-storm clouds: a case study of the dust-storm event of April 1979. Tellus B 35B, 189–196.

Ji, J.J., Liu, Q., Li, Y.P., 2004. Features and simulation of surface water balance in semi-arid areas. Acta geographica sinica 59, 964–971 (in Chinese with English abstract).

Jiang, J.M., Wu, J.L., Shen, J., 2004. Lake sediment records of climatic and environmental change in Angulinao Lake. Scientia Geographica Sinica 24, 346–351 (in Chinese with English abstract).

Jin, Z.D., Wang, S.M., Shen, J., Wang, J., 2000. Dust-storm events in Daihai Lake area, Inner Mongolia during the past 400 years: evidence from grain-size analysis of lake sediments. Journal of Lake Sciences 12, 193–198 (in Chinese with English abstract).

Küster, Y., Hetze, R., Krbetschek, M., Tao, M.X., 2006. Holocene loess sedimentation along the Qilian Shan (China): significance for understanding the processes and timing of loess deposition. Quaternary Science Reviews 25, 114–125.

Lin, T.H., 2001. Long-range transport of yellow sand to Taiwan in spring 2000: observed evidence and simulation. Atmospheric Environment 35, 5873–5882.

Liu, Y.Z., Dong, G.R., Li, C.Z., 1992. Study on some factors influencing soil erosion by wind tunnel experiment. Journal of Desert Research 12, 41–49 (in Chinese with English abstract).

Liu, H.Y., Wang, Y., Tian, Y.H., 2006. Climatic and anthropogenic controls of surface pollen in East Asian steppes. Review of Palaeobotany and Palynology 138, 281–289.

Liu, H.Y., Yin, Y., Tian, Y.H., Ren, J., Wang, H.Y., 2008. Climatic and anthropogenic controls of topsoil features in the semi-arid East Asian steppe. Geophysical Research Letters 35, L04401.

Liu, H.Y., Yin, Y., Zhu, J.L., Zhao, F.J., Wang, H.Y., 2010. How did the forest respond to Holocene climate drying at the forest-steppe ecotone in northern China? Quaternary International 227, 46–52.

Lu, H.Y., Miao, X.D., Zhou, Y.L., Mason, J., Swinehart, J., Zhang, J.F., Zhou, L.P., Yi, S.W., 2005. Late Quaternary aeolian activity in the Mu Us and Otindag dune fields (north China) and lagged response to insolation forcing. Geophysical Research Letters 32, L21716.

Nagashima, K., Tada, R., Matsui, H., Irino, T., Tani, A., Toyoda, S., 2007. Orbital- and millennial-scale variations in Asian dust transport path to the Japan Sea. Palaeogeography, Palaeoclimatology, Palaeoecology 247, 144–161.

Peng, Y.J., Xiao, J.L., Nakamura, T., Liu, B., 2005. Holocene East Asian monsoonal precipitation pattern revealed by grain-size distribution of core sediments of Daihai Lake in Inner Mongolia of north-central China. Earth and Planetary Science Letters 233, 467–479.

Porter, S.C., An, Z.S., 1995. Correlation between climate events in the North Atlantic and China during the last glaciation. Nature 375, 305–308.

Pye, K., 1987. Aeolian Dust and Dust Deposits. Academic Press, London, p. 334.

Pye, K., 1995. The nature, origin and accumulation of loess. Quaternary Science Reviews 14, 653–667.

Qiang, M.R., Chen, F.H., Zhang, J.W., Zu, R.P., Jin, M., Zhou, A.F., Xiao, S., 2007. Grain size in sediments from Lake Sugan: a possible linkage to dust storm events at the northern margin of the Qinghai–Tibetan Plateau. Environmental Geology 51, 1229–1238.

Qiu, W.L., Zhai, Q.M., Hu, H.B., Zhao, Y., Zheng, L.M., Li, R.Q., 1999. Holocene water level changes of Angulinao lake and their environmental significance. Journal of Beijing Normal University (Natural Science) 35, 542–548 (in Chinese with English abstract).

Reimer, P.J., Baillie, M.G.L., Bard, E., Bayliss, A., Beck, J.W., 2004. INTCAL04 terrestrial radiocarbon age calibration, 0–26 cal kyr BP. Radiocarbon 46, 1029–1058.

Ren, G.Y., 1998. A finding of the influence of "Hard Water" on radio carbon dating for lake sediments in Inner Mongolia, China. Journal of Lake Science 10, 80–82 (in Chinese with English abstract).

Shi, P.J., Yan, P., Yuan, Y., 2001. The driving force analyses of the blown-sand activity in Northern China. Quaternary Sciences 21, 41–47 (in Chinese with English abstract).

Shi, P.J., Yan, P., Yuan, Y., 2004. Wind erosion research in China: past, present and future. Progress in Physical Geography 28, 366–386.

Skapura, D.M., 1996. Building Neural Networks. ACM Press, p. 282.

Tsoar, H., Pye, K., 1987. Dust transport and the question of desert loess formation. Sedimentology 34, 139–153.

Van der Baan, M., Jutten, C., 2000. Neural networks in geophysical applications. Geophysics 65, 1032–1047.

Wang, S.M., Dou, H.S., 1998. Lakes of China, 311–312. Science Press, Beijing, p. 545 (in Chinese).

Wang, S.M., Yu, S.Y., Wu, R.J., Feng, M., 1990. The Daihai Lake – lake environment and climate change. China University of Science and Technology Press, Hefei. (in Chinese).

Wang, X.M., Dong, Z.B., Zhang, J.W., Liu, L.C., 2004. Modern dust storms in China: an overview. Journal of Arid Environments 58, 559–574.

Wang, H.Y., Liu, H.Y., Zhu, J.L., Yin, Y., 2010. Holocene environmental changes as recorded by mineral magnetism of sediments from Anguli-nuur Lake, southeastern Inner Mongolia Plateau, China. Palaeogeography, Palaeoclimatology, Palaeoecology 285, 30–49.

Water Bureau of Zhangbei, 2005. Report on the investigation of Lakes, reservoirs, and rivers in the Zhangbei town, 2–8 (unpublished government report).

Water Bureau of Zhangjiakou City, 2005. Report on the investigation of the dessication of the Angulinao Lake, 5–12 (unpublished government report).

Wu, Y.H., Lücke, A., Jin, Z.D., Wang, S.M., Schleser, G.H., Battarbee, R.W., Xia, W.L., 2006. Holocene climate development on the central Tibetan Plateau: a sedimentary record from Cuoe Lake. Palaeogeography, Palaeoclimatology, Palaeoecology 234, 328–340.

Xiao, J., Chang, Z., Si, B., Qin, X., Itoh, S., Lomtatidze, Z., 2009. Partitioning of the grain-size components of Dali Lake core sediments: evidence for lake-level changes during the Holocene. Journal of Paleolimnology 42, 249–260.

Yang, S.L., Ding, Z.L., 2008. Advance–retreat history of the East-Asian summer monsoon rainfall belt over northern China during the last two glacial–interglacial cycles. Earth and Planetary Science Letters 274, 499–510.

Yasunari, T.J., Yamazaki, K., 2009. Impacts of Asian dust storm associated with the stratosphere-to-troposphere transport in the spring of 2001 and 2002 on dust and tritium variations in Mount Wrangell ice core, Alaska. Atmospheric Environment 43, 2582–2590.

Zhai, Q.M., Li, R.Q., 2002. Annual laminations of grain size in Angulinuo Lake and the environmental changes in Bashang Plateau. Scientia Geographica Sinica 22, 331–335 (in Chinese with English abstract).

Zhai, Q.M., Guo, Z.Y., Li, Y.L., Li, R.Q., 2006. Annually laminated lake sediments and environmental changes in Bashang Plateau, North China. Palaeogeography, Palaeoclimatology, Palaeoecology 241, 95–102.

Zhang, D.E., 1984. A preliminary analysis of climatology of the dustfall in the history in China. Science in China Series B 24, 278–288.

Zhang, Y.K., 2010. Drivers of lake water area reduction and dessication in semi-arid region of China over the last 40 years. *Master thesis of Peking University*, 74–86 (in Chinese with English abstract).

Zhang, D.E., Lu, F., 1999. Winter sandstorm events in extensive Northern China. Quaternary Sciences 5, 441–447 (in Chinese with English abstract).

Zhao, Y., Yu, Z.C., Chen, F.H., Zhang, J.W., Yang, B., 2009. Vegetation response to Holocene climate change in monsoon-influenced region of China. Earth-Science Reviews 97, 242–256.